Edelweiss Applied Science and Technology
ISSN: 2576-8484
Vol. 9, No. 4, 1176-1189
2025
Publisher: Learning Gate
DOI: 10.55214/25768484.v9i4.6223

Vibration-based structural anomaly detection and health monitoring of urban air mobility vehicles

Soeng-Weon Seo[1], Dong-Gi Kwag[1,2*]
[1]Department of Aeronautical System Engineering, Hanseo University, Taean 32158, Korea; seo7160@naver.com (S.W.S.)
[2]Department of Aero Mechanical Engineering, Hanseo University, Taean 32158, Korea; dgkwag@hanseo.ac.kr (D.G.K.).

Abstract: The urban air mobility (UAM) market continues to grow as the importance of structural health monitoring (SHM) technology is increasingly emphasized for safe operation. This study proposes a Euclidean distance vector-based vibration analysis method for the early detection of abnormal vibrations and for performing safety diagnostics in the rotor-arm system of a multicopter-type UAM. Vibration experiments were conducted by simulating abnormal conditions such as mass imbalance, bolt loosening, and propeller damage in stages to verify this approach, thereby reflecting actual operating environments. The frequency response and vibration characteristics were analyzed in comparison to normal conditions. The analysis showed that even minor mass imbalances and bolt loosening caused a significant increase in vibration within specific frequency bands. Certain frequency bands exhibited pronounced damping effects as damage worsened, revealing complex dynamic behavior. These results confirm shifts in resonance frequency and dispersion of vibration energy due to structural dynamic changes, thereby demonstrating the effectiveness of the Euclidean distance vector-based analysis method in detecting such anomalies. In conclusion, the proposed method enables the early detection of anomalies in multicopter-type UAM rotor arms, providing a basis for safety diagnostics and potentially enhancing reliability through expansion into fault detection systems.

Keywords: *Urban air mobility, Vibration test, health monitoring, Airframe defect, Safety evaluation, Euclidean distance, Personal air vehicle.*

1. Introduction

Urban air mobility (UAM) vehicles require high structural reliability to ensure safe operation in complex urban airspace. In fact, 64% of the Uinted States Air Force unmanned aerial vehicle system accidents have been attributed to mechanical failures, highlighting the urgency to develop technologies that can detect and quantitatively assess anomalies at an early stage [1]. Rotational imbalances caused by propeller damage, mass imbalance, and fastening defects, which have been previously reported in wind turbines and aircraft engines, are key factors that can alter natural frequencies and amplitudes, thereby making them critical references for UAM vibration analysis [2-4]. These rotational imbalances can induce structural vibrations that can act as key determinants of UAM operational conditions. Conventional structural health monitoring (SHM) technologies focus on detecting damage only in static structures, which makes their real-time adaptation to dynamic environments, such as those in high-speed aircraft and UAMs, challenging [5]. Traditional monitoring techniques used in bridges and buildings are well-suited for periodic inspections, whereas aircraft and UAMs require immediate responses to rapidly changing stress and environmental factors, necessitating advanced analytical approaches [6, 7]. In this context, research studies on methods that can assess real-time fatigue and deformation characteristics and prevent defect propagation are gaining attention as a crucial approach toward ensuring the operational safety of aircraft and UAMs [8].

History: Received: 11 February 2025; Revised: 28 March 2025; Accepted: 2 April 2025; Published: 14 April 2025
* Correspondence: dgkwag@hanseo.ac.kr

This study proposes an analysis method to identify anomalies early using a multicopter-type UAM rotor-arm system. Theoretical modeling, finite element analysis (FEA), and experimental data are compared to analyze vibration characteristics for ensuring the reliability of the proposed method. Vibration data from the rotor-arm system of a multicopter-type UAM are collected and categorized by frequency bands to confirm the effectiveness of detecting anomalies such as mass imbalance, propeller damage, and fastening defects. Integrating this analytical method with SHM technology can aid in the development of pre-flight inspection and real-time monitoring systems, which can enhance UAM safety and reliability. The consistency of the vibration experiment results is verified and used to compare the vibration characteristics of normal and abnormal states.

SHM has been widely employed in various fields, including aircraft, automobiles, bridges, and high-rise buildings. Advances in sensor technology, combined with big data and artificial intelligence, have enabled more precise and reliable monitoring. These technologies play a crucial role in real-time structural monitoring, early detection of potential defects, and ensuring maintenance and safety [8, 9].

In the UAM sector, SHM is gaining increasing importance for the efficient management of the complex structures of aircraft such as electric vertical takeoff and landing (eVTOL). Further, SHM analyzes the data collected from sensors (structural vibrations, stress, and deformation) to detect or predict structural issues. Unlike previous SHM studies that utilized various state variables of normal systems and applied weights based on covariance magnitude to enhance system differentiation through complex distance calculation methods, this study proposes a simplified approach that uses the vibration signal spectrum from a multicopter-type UAM rotor-arm as a single variable and evaluates UAM safety using Euclidean distance vectors [10-14]. The proposed method is computationally efficient and effective in diagnosing propeller anomalies. Designed with limited memory and computational constraints for flight and attitude control, the proposed approach can enhance UAM safety and contribute to the reliability and performance of eVTOL and similar UAM platforms.

2. Main Discussion

2.1. Equivalent Model and Finite Element Analysis of UAM Rotor-Arm

2.1.1. Equivalent Model of UAM Rotor-Arm

Material properties such as density and elastic modulus required to calculate natural frequencies were obtained through measurements, and experiments were conducted to apply these FEA to the equivalent model of a multicopter-type UAM rotor-arm. A cantilever beam model, which is widely used to study the vibration characteristics of aircraft wings and rotary blades, was considered suitable for analyzing the UAM rotor-arm and applied in the equivalent modeling process [15].

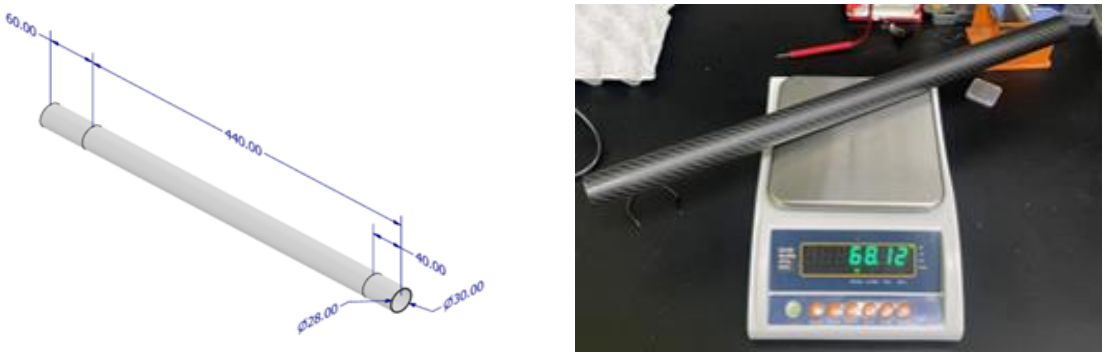

(a) (b)

Figure 1.
(a) 3D CAD image of a circular cross-section cantilever beam, (b) Measured weight.

Edelweiss Applied Science and Technology
ISSN: 2576-8484
Vol. 9, No. 4: 1176-1189, 2025
DOI: 10.55214/25768484.v9i4.6223

Figures 1(a) and 1(b) show that the circular cross-section cantilever beam was measured and modeled using a 3D CAD(Computer-Aided Design) program to calculate its volume and the actual measured weight of the circular cross-section cantilever beam, which was used to calculate its density, respectively. In addition, the Young's modulus of the circular cross-section cantilever beam material was determined using its deflection. A weight was applied, and the deflection was measured with a laser displacement sensor. This calculation was performed using [15].

$$E = \frac{PL^3}{3\,\delta I} \quad (1)$$

where E, P, L, I, and δ represent the elastic modulus of the beam, weight of the mass load, length of the beam, moment of inertia about the z-axis, and deflection of the beam when the mass load is applied, respectively.

Experimental results for the material properties of the circular cantilever beam showed a density of 1493 kg/m^3 and Young's modulus of 1.86 GPa. These values were applied to the equivalent model and FEA analysis, as shown in Figure 2(b). The circular cross-section cantilever beam was modeled as an equivalent structure.

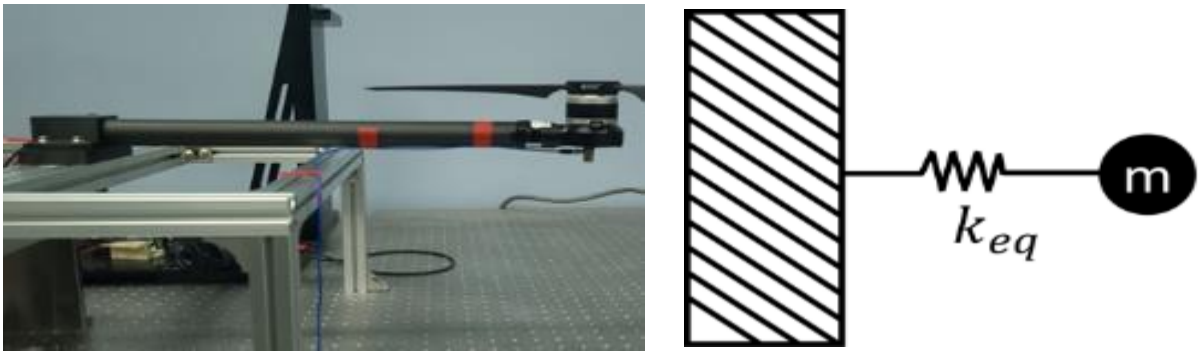

(a) (b)

Figure 2.
(a) Experimental setup of UAM rotor-arm and (b) equivalent modeling.

Figure 2(a) shows the experimental setup for the vibration analysis of the UAM rotor-arm. Considering real operational conditions, one end of the rotor-arm was fixed using a jig, which formed a cantilever beam structure. Sensors were installed near the motor center for effectively analyzing vibrations generated during rotor rotation to accurately measure vibration characteristics. Figure 2(b) represents an undamped single-degree-of-freedom system, where the cantilever beam structure was simplified into an equivalent stiffness model. In this model, the equivalent stiffness k_{eq} reflects the geometric and material properties of the cantilever beam, and the theoretical solution for the natural frequency is given by Rao [16].

$$\omega = \sqrt{\frac{3EI}{mL^3}} \quad (2)$$

where ω, E, m, I, and L represent natural frequency, elastic modulus, second moment of area, weight of the rotor, and length of the beam, respectively.

2.1.2. Finite Element Analysis of UAM Rotor-Arm

This study utilized the program Ansys 2019 R3 to conduct a modal analysis and derive natural frequencies to perform the FEA of the UAM rotor-arm. Boundary conditions and mesh settings were applied to obtain reliable data for comparison with experimental results. The tetrahedral meshing method was used for mesh generation, thereby resulting in a total of 77,916 elements. More than 50% of the elements had a quality factor above 0.73, which helped ensure the reliability of the mesh for the

Edelweiss Applied Science and Technology
ISSN: 2576-8484
Vol. 9, No. 4: 1176-1189, 2025
DOI: 10.55214/25768484.v9i4.6223

FEA.

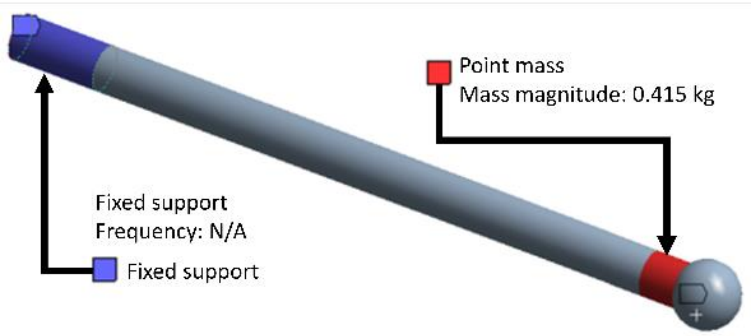

Figure 3.
Boundary conditions of the UAM rotor-arm.

Figure 3 illustrates boundary conditions applied in the FEA analysis of the UAM rotor-arm. The fixed support boundary condition was applied to the jig-fixed section. In addition, the mass of the rotor and propeller was modeled as a point mass at the free end of the cantilever beam.

Table 1.
Theoretical solutions and FEA errors for the natural frequencies of the multicopter-type UAM rotor-arm.

Mode	Theoretical solution	Finite element analysis	Error rate
First mode	18.9 Hz	19.1 Hz	1.0%
Second mode	424.8 Hz	448.5 Hz	5.2%

Table 1 presents theoretical solutions and FEA results for the natural frequencies of the UAM rotor-arm. The comparison shows that the multicopter-type UAM rotor-arm exhibited error rates of 1.0 and 5.2% in the first and second modes, respectively. This indicates that the measured material properties of the UAM rotor-arm are reliable. In addition, natural frequencies identified in Table 1 serve as reference frequencies for normal conditions in vibration testing.

2.2. Experiment Setup

2.2.1. Impact Hammer Vibration Experiment Setup

An impact hammer vibration experiment was conducted to verify the natural frequencies of the multicopter-type UAM rotor-arm and confirm its normal-state characteristics. The experiment was performed on an anti-vibration table to minimize the effect of external noise and vibrations. The collected experimental data were used to analyze the dynamic characteristics of the system and compared with FEA results.

Before presenting the results, it is important to describe the methodology and significance of the test. The impact hammer test is a vibration testing method used for evaluating and analyzing the dynamic characteristics of the system. In this study, the test was conducted to determine the rotor-arm's natural frequencies, serving as a reference for vibration assessments in later experiments.

Edelweiss Applied Science and Technology
ISSN: 2576-8484
Vol. 9, No. 4: 1176-1189, 2025
DOI: 10.55214/25768484.v9i4.6223

Figure 4.
Architecture of the impact hammer experiment.

Figure 4 shows the experimental setup for the impact hammer vibration test of the multicopter-type UAM rotor-arm. To ensure consistency, the UAM rotor-arm was struck ten times at a designated impact point using an impact hammer, and the frequency response function curve was derived from the averaged results. This process applied a physical impact similar to a unit impulse function, and the response of the system was measured, transformed, and analyzed as a response function [17].

The Federal Aviation Administration has established UAM certification standards based on the safety regulations of conventional light aircraft and helicopters. In accordance with MIL-STD-810H, which defines vibration testing for light aircraft and helicopters, the frequency range of interest was set between 1 and 1,000 Hz. Consequently, this experiment collected data at a sampling rate of 2,000 Hz, allowing analysis up to 1,000 Hz. Data were processed using a data acquisition system, with a resolution of 0.1 Hz for graphical fitting [18, 19].

2.2.2. Rotor Rotation Vibration Experiment setup

To analyze the impact of abnormal conditions on rotor vibration characteristics, experiments were conducted by simulating three key scenarios: mass imbalance, bolt loosening, and propeller damage. The motor rotation speed was set to 1,000 rpm (~16.6 Hz), and data collection began after a two-minute stabilization period to establish a consistent baseline. The collected data were then transformed into the frequency domain using the fast Fourier transform (FFT). To enhance the clarity of frequency analysis, the 1,000 Hz range was segmented into ten frequency bands at 100 Hz intervals, ensuring efficient identification of resonance patterns and anomalies.

2.2.3. Mass Imbalance Simulation

1. Mass imbalance in the propeller was simulated to replicate real-world scenarios where foreign substances such as moisture, dust, or ice accumulate on the propeller during operation.

Figure 5.
Image of propeller mass imbalance experiment condition.

Figure 5 illustrates the experimental setup, where additional mass was attached to the propeller tip. The experiment simulated mass imbalance conditions using 0.2 g and1.0 g weights. To create an

Edelweiss Applied Science and Technology
ISSN: 2576-8484
Vol. 9, No. 4: 1176-1189, 2025
DOI: 10.55214/25768484.v9i4.6223

intentional center of mass shift, a designated weight was affixed to the tip of the propeller blade (marked with a red dashed line). This setup enabled an assessment of how mass imbalance affects the rotational and vibrational characteristics of the rotor system.

2.3. Bolt Loosening Simulation

To examine the effects of bolt loosening on structural stability, an experiment was conducted where propeller hub securing bolts were intentionally loosened to simulate progressive weakening due to continuous vibrations during UAM operation.

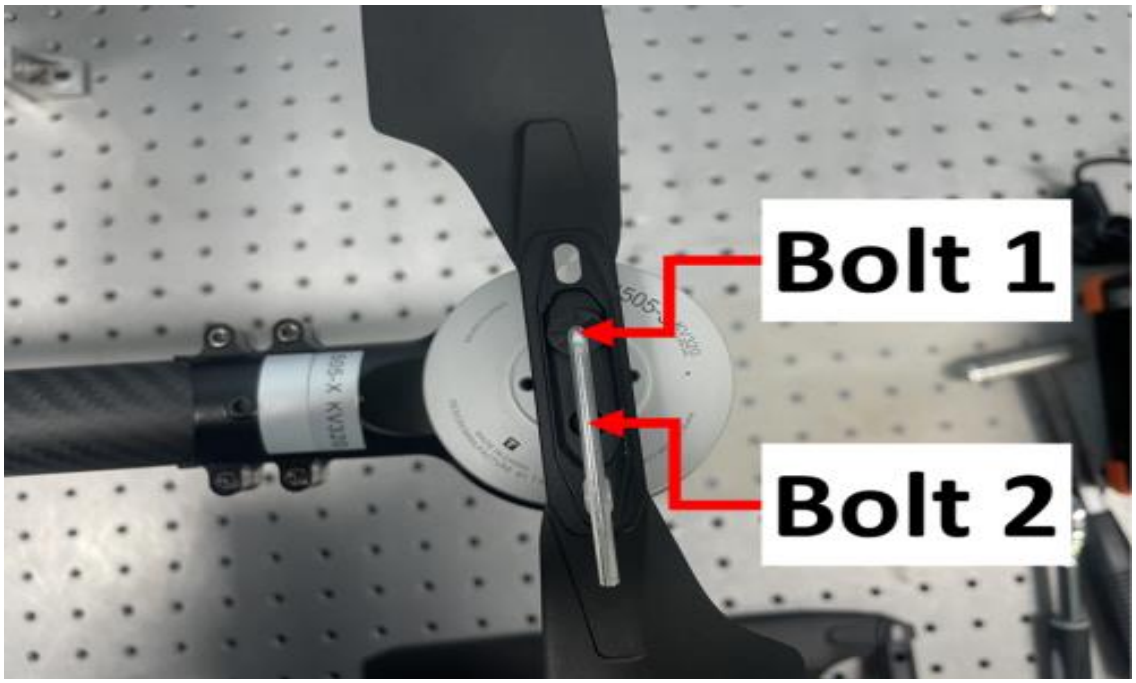

Figure 6.
Bolt positions in bolt loosening experiment.

As shown in Figure 6, bolt 1 of the propeller hub was loosened by ½ pitch and 1 pitch before conducting the rotation test. The experiment aimed to determine how prolonged vibrations impact bolt fastening strength and evaluate the corresponding effects on structural stability and vibration characteristics.

2.4. Propeller Damage Simulation

To simulate real-world scenarios where propeller damage occurs during UAM operation, an experiment was designed to analyze dynamic behavior and vibration characteristics under varying levels of propeller damage. Figure 7 presents the experimental setup for propeller damage simulation. To ensure controlled test conditions, the propeller blade was deliberately cut to introduce predefined damage conditions.

Edelweiss Applied Science and Technology
ISSN: 2576-8484
Vol. 9, No. 4: 1176-1189, 2025
DOI: 10.55214/25768484.v9i4.6223

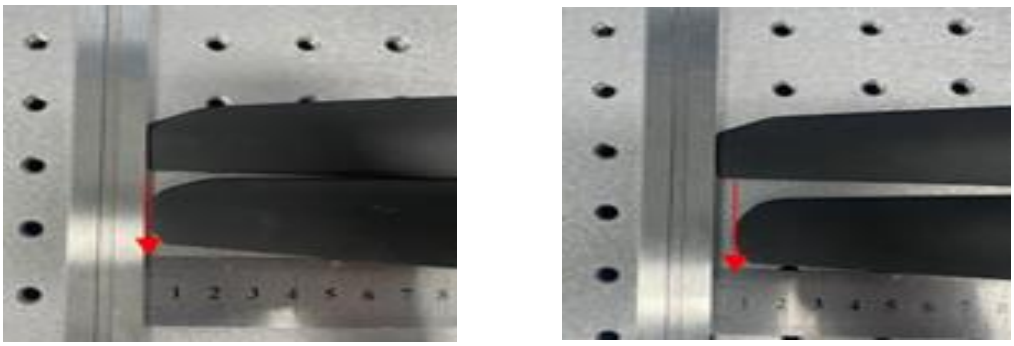

(a) (b)

Figure 7.
Experiment condition images of (a) 1 and (b) 5 mm propeller damage.

Figure 7(a) represents a minor damage case with a 1 mm cut, while Figure 7(b) simulates a more severe 5 mm damage condition. The impact of propeller damage on rotational balance and overall dynamic performance was evaluated to assess how different levels of damage influence structural stability.

2.5. Verification Experiment of Natural Frequencies and Normal Condition

The following experiment was conducted to measure and verify the natural frequencies of the UAM rotor-arm. The obtained results were then compared with FEA predictions to ensure accuracy.

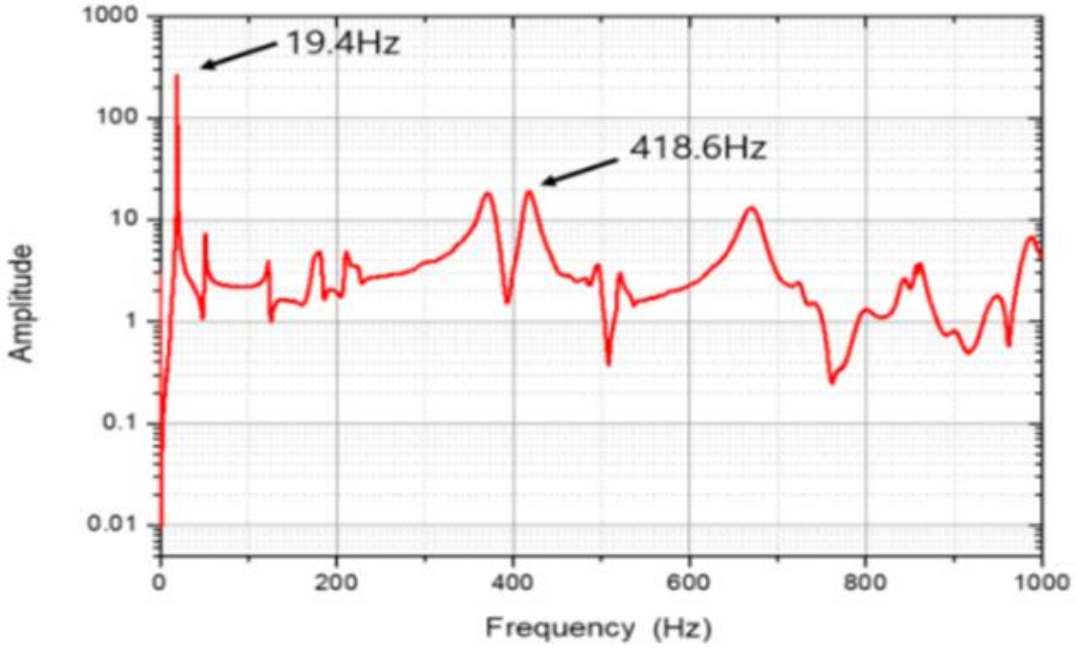

Figure 8.
Impact hammer experiment results.

Edelweiss Applied Science and Technology
ISSN: 2576-8484
Vol. 9, No. 4: 1176-1189, 2025
DOI: 10.55214/25768484.v9i4.6223

Figure 8 presents the results of the impact hammer experiment. Through this experiment, the natural frequencies of the UAM rotor-arm were identified, and the obtained results were compared with previously conducted FEA results for calculating the error rate. The analysis results are presented in Table 2.

Table 2.
Comparison of Finite Element Analysis and Impact Hammer Experiment.

Mode	Finite Element Analysis	Impact Hammer	Error Rate
First mode	19.1 Hz	19.4 Hz	1.57%
Second mode	448.8 Hz	418.6 Hz	7.21%

Table 2 presents a comparison of the impact hammer experiment and FEA results. The experimental results showed that, within the 1,000 Hz range, the maximum error rate compared to FEA was 7.21%, confirming the reliability of the experimental setup. The derived natural frequencies serve as reference frequencies for normal conditions in vibration testing and as a basis for the early detection of structural anomalies in actual operational environments.

2.6. UAM Rotor-Arm Normal and Abnormal Condition Rotor Rotation Vibration Experiment and Analysis

In this studyThe top five peak values were selected for analysis to reduce interference between rotor harmonic components and noise in each frequency segment.

$$d(p,q) = \sqrt{\sum_{i=1}^{n}(p_i - q_i)^2} \quad (3)$$

$$T_{95\%} = \mu \pm 1.96\sigma \quad (4)$$

where p_i, q_i, n, $T_{95\%}$, μ, and σ represent the top peak values measured under normal conditions, top peak values measured under abnormal conditions, number of peak values in each frequency band, confidence interval (95%), average distance between normal and abnormal state vectors, and standard deviation of distance values, respectively.

In this study, Euclidean distance vectors were used for data analysis and vibration pattern classification. The Euclidean distance vector calculates the distance between top peak values in each segment under normal conditions (p_i) and corresponding peak values (q_i) in the signal being analyzed. This is expressed as Equation (3). This approach is highly effective in detecting anomalies early by quantitatively distinguishing between normal and abnormal states [20]. A threshold based on the 95% confidence interval (Equation 4) was used for systematically determining the presence of abnormalities [21]. This method ensures reliable vibration analysis by effectively responding to noise and load fluctuations that can occur in real-world operational environments.

2.6.1. Propeller Normal Condition Rotor Rotation Experiment

Prior to analyzing abnormal vibration characteristics, experiments were first conducted under normal conditions to establish a baseline reference. Three repeated experiments were conducted under normal conditions to compare normal and abnormal conditions, and the data were analyzed using Euclidean distance vectors. The normal condition was defined as the state in which the propeller and bolts were intact and securely fastened to the rotor before operation.

Edelweiss Applied Science and Technology
ISSN: 2576-8484
Vol. 9, No. 4: 1176-1189, 2025
DOI: 10.55214/25768484.v9i4.6223

Table 3.
Normal condition Euclidean distance comparison (Unit: dB)

Category	Segment									
	1	**2**	**3**	**4**	**5**	**6**	**7**	**8**	**9**	**10**
Case 1	8.6	5.2	8	4.1	2.7	2.1	2.9	4.9	3.7	3.3
Case 2	7.9	1.6	2.2	2.9	3.4	3.1	3.2	7	2.8	3.5
Case 3	9.3	1.9	4.5	6.6	3.2	2.4	4.6	5.7	2.2	3
μ	8.6	2.9	4.9	4.53	3.1	2.53	3.57	5.87	2.9	3.27
σ	0.7	2	2.92	1.89	0.36	0.51	0.91	1.06	0.75	0.25

Table 3 lists the Euclidean distance vector results for each frequency segment derived from three repeated experiments (Cases 1, 2, and 3) under normal conditions, along with the mean (μ) and standard deviation (σ). The threshold range for Euclidean distances in normal conditions is defined based on these results. If the Euclidean distance vector value measured in the abnormal condition vibration test exceeds this threshold, it indicates a deviation from the normal operational range and suggests an abnormal state.

2.6.2. Propeller Mass Imbalance Simulation Rotor Rotation Experiment

To investigate the effects of mass imbalance, an experimental study was conducted by attaching additional weights to the propeller.

Table 4.
Propeller mass imbalance experiment distance vector comparison.

Category		Segment									
Weight (g)	**Experiment**	**1**	**2**	**3**	**4**	**5**	**6**	**7**	**8**	**9**	**10**
0.2	1	7.6	8.4	5.4	12	16.7	1.2	7	20.7	12.4	6.3
	2	7.9	8	5.9	12.5	17	1.5	7.2	20.2	12.8	6.5
	3	8.2	7.9	6.1	12.4	17	1.5	7.1	20.3	12.9	6.7
	Mean	7.9	8.1	5.8	12.3	16.9	1.4	7.1	20.4	12.7	6.5
1.0	1	12.1	1.6	4	4	14.9	19.5	4.8	10.3	6.9	12.9
	2	11.1	2.3	3.2	4.4	15	22.5	4.7	12.4	6.1	10.5
	3	10.4	2.4	3.3	6	12.4	22.2	5.2	11.5	5.3	15.9
	Mean	11.2	2.1	3.5	4.8	14.1	21.4	4.9	11.4	6.1	13.1

Table 4 lists the results of the mass imbalance experiment. When an additional mass of 0.2 g was attached, significant vibration amplification occurred in specific frequency segments (2, 4, 5, 8, 9, and 10), and strong resonance phenomena were observed even with a relatively small mass change. This indicates that minor mass variations can significantly affect the dynamic stability of the system within specific frequency bands. In contrast, the average vibration intensity was not always greater than in the 0.2 g condition when an additional mass of 1.0 g was attached, vibrations exceeding the normal state range were observed in most frequency segments. This implies that the increase in mass caused shifts in natural frequencies and led to a complex combination of vibration amplification and damping.

2.6.3. Propeller Bolt Loosening Simulation Rotor Rotation Experiment

To evaluate the impact of bolt loosening on vibration characteristics, an experiment was conducted where the propeller hub securing bolts were deliberately loosened to simulate progressive weakening caused by continuous vibration exposure.

Edelweiss Applied Science and Technology
ISSN: 2576-8484
Vol. 9, No. 4: 1176-1189, 2025
DOI: 10.55214/25768484.v9i4.6223

Table 5.
Bolt loosening experiment distance vector comparison.

Experiment		Segment									
Variables	Number	1	2	3	4	5	6	7	8	9	10
½ pitch	1	8.7	8.3	0.8	15.5	9.2	22.4	10.8	17.2	23.8	10.5
	2	8.9	8.2	2.8	16.5	8.6	21	11.5	14.9	23.8	12.2
	3	10	9	2.1	17.2	11.9	19	11.6	14.9	23.2	10.9
	Mean	9.2	8.5	1.9	16.4	9.9	20.8	11.3	15.7	23.6	11.2
1 pitch	1	6.8	1.2	2.9	7.9	8.5	6.3	7	33.2	24.8	5.3
	2	8	0.2	3.7	10.7	6	10.7	8.5	33	25.5	3.7
	3	7.4	1.6	4.8	6.6	6.2	7.3	5.8	33.4	26.1	5.1
	Mean	7.4	1	3.8	8.4	6.9	8.1	7.1	33.2	25.5	4.7

Table 5 presents the Euclidean distance vector calculation results from the bolt loosening experiment. When the bolt was loosened by 1/2 pitch, significant vibration amplification was observed in all frequency segments except segments 1 and 3, implying that the partial loss of fastening strength had a major impact on resonance phenomena in specific frequency bands. In contrast, when the bolt was loosened by 1 pitch, exceptionally high vibration intensity exceeding the normal range was observed in certain frequency segments (particularly segments 5, 6, 8, and 9). This confirms that a significant reduction in fastening strength can severely affect the overall dynamic stability of the system.

2.6.4. Propeller Damage Simulation Rotor Rotation Experiment

To investigate the effects of propeller damage on vibration characteristics, an experimental study was conducted where controlled damage was introduced to the propeller blade.

Table 6.
Propeller damage experiment distance vector comparison.

Experiment		Segment									
Variables	Number	1	2	3	4	5	6	7	8	9	10
1 mm	1	9.9	4.3	2.4	7.5	10.7	12.8	10.8	12.9	5.4	10.1
	2	7.4	5	2.8	10.7	7.1	13.7	9.6	12	4.1	9.7
	3	6.7	4.8	3.7	9.1	8.6	14	11.6	14	3.3	7.9
	Mean	8	4.7	3	9.1	8.8	13.5	10.7	13	4.3	9.2
5 mm	1	12.5	2.1	4.9	8.8	13.9	9.1	16.6	24.7	11.7	7
	2	8.8	2	4.2	9.4	16.3	4.2	15.2	24	11.5	8.1
	3	10.5	2.4	5	11.2	18.7	11	14.7	25.4	11	5.3
	Mean	10.6	2.2	4.7	9.8	16.3	8.1	15.5	24.7	11.4	6.8

Table 6 lists the Euclidean distance vector calculation results from the propeller damage experiment. In the 1 mm damage condition, vibration amplification was clearly observed in certain frequency segments (particularly 5, 6, 7, 8, and 10) compared to those of normal conditions. This indicates that even minor damage can induce resonance phenomena in specific frequency bands. In contrast, in the 5 mm damage condition, a high level of vibration was observed; however, damping effects were noted in some segments (particularly 2 and 10). This implies that severe damage may exhibit complex dynamic behavior by redistributing vibrational energy into different modes.

Edelweiss Applied Science and Technology
ISSN: 2576-8484
Vol. 9, No. 4: 1176-1189, 2025
DOI: 10.55214/25768484.v9i4.6223

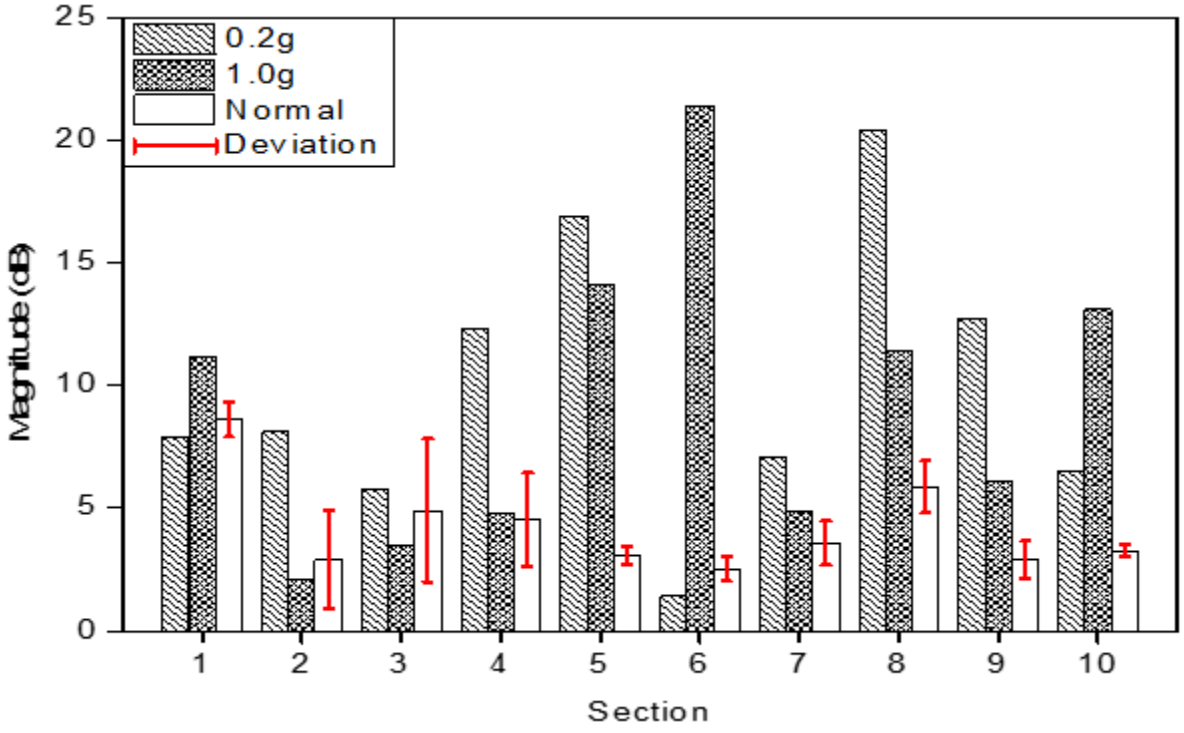

(a)

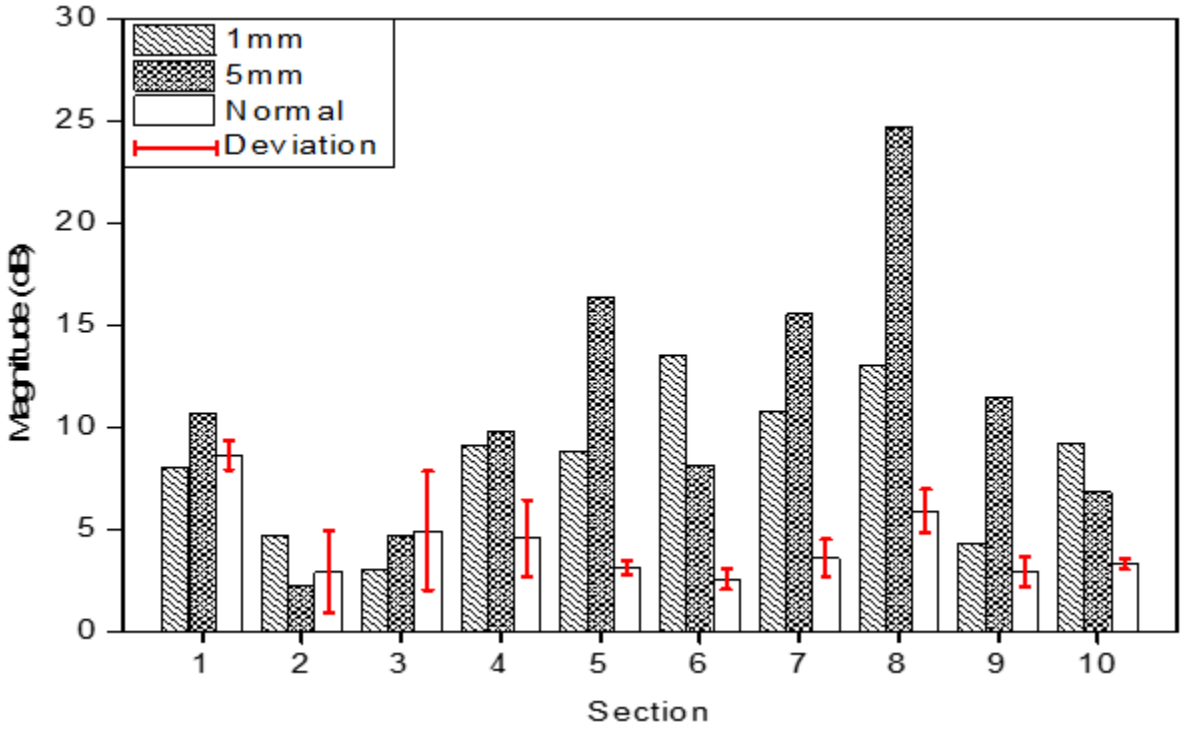

(b)

Edelweiss Applied Science and Technology
ISSN: 2576-8484
Vol. 9, No. 4: 1176-1189, 2025
DOI: 10.55214/25768484.v9i4.6223

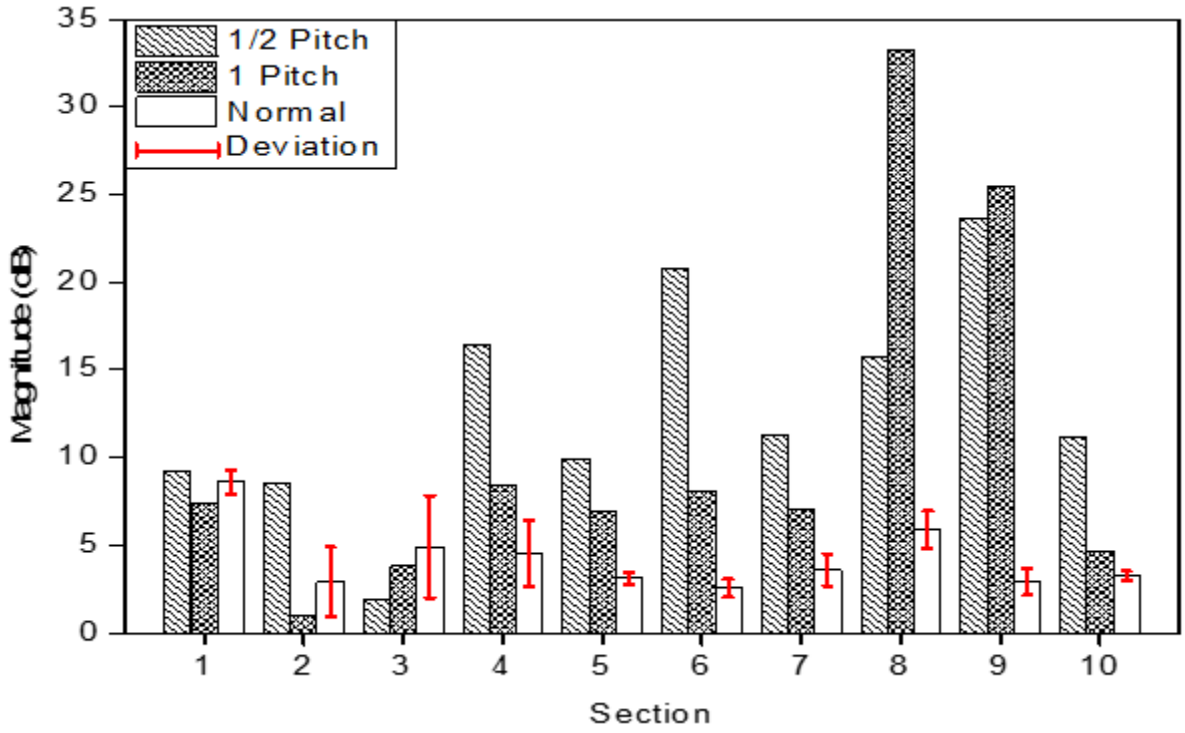

(c)

Figure 9.
Comparative graphs of normal and abnormal conditions across frequency segments: (a) Mass imbalance, (b) bolt loosening, and (c) propeller damage.

Figure 9 displays graphs showing the mean and standard deviation of vibration intensity across frequency segments for normal and various abnormal conditions (mass imbalance, bolt loosening, and propeller damage). A comparison of normal and abnormal conditions revealed that in all abnormal cases, certain frequency segments (particularly 5, 8, 9, and 10) exhibited a distinct increase in vibration intensity compared to those in normal conditions. This suggests the occurrence of resonance phenomena near the natural frequencies of the structure.

In the mass imbalance experiment shown in Figure 9(a), even a small additional mass of 0.2 g caused significant vibration amplification in segments 2, 4, 5, 8, 9, and 10, suggesting strong resonance effects. In contrast, with 1.0 g attached, the average vibration intensity was not always higher than that in the 0.2 g condition; however, a broader dispersion was observed across multiple segments, implying a complex interaction of natural frequency shifts and vibration amplification caused by increased mass.

In the bolt loosening experiment shown in Figure 9(b), the 1/2 pitch loosening condition exhibited significant vibration amplification in all frequency segments except 1 and 3, implying that reduced fastening strength had a major effect on those frequency bands. Under the 1 pitch loosening condition, vibration intensity significantly exceeded the normal range in specific frequency segments (particularly 5, 6, 8, and 9), suggesting that a substantial decrease in fastening strength could severely affect the overall dynamic characteristics of the system.

In the propeller damage experiment shown in Figure 9(c), the 1 mm damage condition led to pronounced resonance amplification in segments 5, 6, 7, 8, and 10, demonstrating that even minor damage can significantly affect specific frequency bands. In the 5 mm damage condition, a high vibration level was observed; however, damping effects occurred in segments 2 and 10, suggesting that severe damage may cause complex behavior by redistributing vibration energy into different modes.

In conclusion, all abnormal conditions exhibited a combination of amplification and damping effects

Edelweiss Applied Science and Technology
ISSN: 2576-8484
Vol. 9, No. 4: 1176-1189, 2025
DOI: 10.55214/25768484.v9i4.6223

across specific frequency segments. Mass imbalance and bolt loosening induced resonance effects that had a significant effect on certain frequency bands, whereas the degree of propeller damage resulted in nonlinear behavior. These findings clearly demonstrate that anomalies in the multicopter rotor-arm system cannot be explained solely by increased vibration. Instead, they involve shifts in natural frequencies and changes in frequency-specific mode characteristics, which leads to complex effects. Therefore, future assessments of structural safety and the development of predictive maintenance systems involve the quantitative analysis of resonance and damping phenomena across frequency segments.

3. Conclusion

This study developed a vibration analysis technique for the SHM of multicopter-type UAMs and proposed a methodology for the early anomaly detection and quantitative evaluation of drive system faults. Fault scenarios such as mass imbalance, bolt loosening, and propeller damage were systematically simulated using a multicopter-type UAM rotor-arm system, and the effectiveness of the Euclidean distance vector-based vibration analysis method was validated. Vibration characteristics were analyzed by dividing the 1,000 Hz range into ten frequency segments at 100 Hz intervals. The results confirmed that even minor anomalies led to a sudden increase in vibration magnitude in specific frequency bands. In addition, certain frequency segments exhibited damping effects as abnormal conditions worsened, indicating complex dynamic behavior. These findings suggested that structural dynamics must be comprehensively considered, including natural frequency shifts, mode changes, and energy redistribution. Further, they highlight the need for quantifying structural changes beyond simple vibration amplification. Even minor propeller damage (1 mm) resulted in resonance amplification in specific frequency bands, while severe damage (5 mm) caused damping effects in some bands, thereby confirming the presence of nonlinear behavior with concurrent resonance and damping. These results demonstrate that the Euclidean distance vector-based analysis method is effective for early anomaly detection and provides a quantitative diagnostic criterion for multicopter-type UAMs. In addition, this study suggested that the proposed method has potential for real-time monitoring and preventive maintenance systems under various operational conditions and environmental factors (e.g., variations in operating RPM, propeller shape, and material properties).

However, this study focused on limited experimental conditions and variables, thereby leaving external factors that may arise in real-world operations (e.g., temperature fluctuations, humidity) as future research topics. In addition, further research on sensor placement strategies and data processing methods need to be conducted to enhance the integration feasibility of the proposed method into actual UAM systems.

Transparency:

The authors confirm that the manuscript is an honest, accurate, and transparent account of the study; that no vital features of the study have been omitted; and that any discrepancies from the study as planned have been explained. This study followed all ethical practices during writing.

Acknowledgements:

This paper was supported by the Hanseo University Internal Research Support Project in 2024.

References

[1] W. Park, "A study on the safety management of UAS by analyzing its accident factors," *Journal of the Korean Society for Aeronautical and Space Sciences*, vol. 31, no. 1, pp. 1–10, 2023. https://doi.org/10.12985/ksaa.2023.31.1.001

[2] X. Jin, X. Ding, Y. Gong, N. Wu, and H. Yan, "Rotor imbalance detection and quantification in wind turbines via vibration analysis," *Wind Engineering*, vol. 46, no. 1, pp. 3-11, 2022. https://doi.org/10.1177/0309524X21999841

[3] T. Xu, Y. Jin, and J. Xu, "Aero-engine vibration fault diagnosis based on harmonic Wavelet," *Advanced Materials Research*, vol. 490, pp. 218-222, 2012. https://doi.org/10.4028/www.scientific.net/amr.490-495.218

[4] C. Skliros, "A case study of vibration fault diagnosis applied at Rolls-Royce T-56 turboprop engine," *Aviation*, vol. 23, no. 3, pp. 78-82, 2019. https://doi.org/10.3846/aviation.2019.11900

[5] B. Bhowmik, T. Tripura, B. Hazra, and V. Pakrashi, "Real time structural modal identification using recursive canonical correlation analysis and application towards online structural damage detection," *Journal of Sound and Vibration*, vol. 468, p. 115101, 2020. https://doi.org/10.1016/j.jsv.2019.115101

[6] A. A. Broer, R. Benedictus, and D. Zarouchas, "The need for multi-sensor data fusion in structural health monitoring of composite aircraft structures," *Aerospace*, vol. 9, no. 4, p. 183, 2022. https://doi.org/10.3390/aerospace9040183

[7] J. Dodson *et al.*, "High-rate structural health monitoring and prognostics: An overview," *Data Science and Engineering*, vol. 9, pp. 213–217, 2022. https://doi.org/10.1007/978-3-030-76004-5_23

[8] G. Sauti, R. A. Wincheski, C. J. Stelter, M. R. Horne, J. P. Moore, and E. J. Siochi, "Enhancing in-flight structural health monitoring of vertical lift vehicles operating in an urban environment.," in *Proceeding 6th Decennial VFS Aeromech. Specialists' Conference, NASA Langley Research Center*, 2024, pp. 1-10.

[9] G. Wild, L. Pollock, A. K. Abdelwahab, and J. Murray, "The need for aerospace structural health monitoring," *International Journal Prognost Health Management*, vol. 12, no. 3, p. 2368, 2021. https://doi.org/10.36001/IJPHM.2021.v12i3.2368

[10] L. Li, A. Brügger, R. Betti, Z. Shen, and L. Gan, "Vibration-based structural damage localization through a discriminant analysis strategy with cepstral coefficients," *Structural Health Monitoring*, vol. 23, no. 6, pp. 3921-3942, 2024. https://doi.org/10.1177/14759217241231034

[11] G. V. Joseph and V. Pakrashi, "Spiking neural networks for structural health monitoring," *Sensors*, vol. 22, no. 23, p. 9245, 2022. https://doi.org/10.3390/s22239245

[12] M. M. Rosso, A. Aloisio, R. Cucuzza, D. P. Pasca, G. Cirrincione, and G. C. Marano, "Structural health monitoring with artificial neural network and subspace-based damage indicators," presented at the International Conference Trends Constr. Post-Dig. Era, Cham: Springer International Publishing, 2022.

[13] A. Deraemaeker and K. Worden, "On the use of the Mahalanobis squared-distance to filter out environmental effects in structural health monitoring," presented at the MATEC Web Conference, 2014.

[14] C. R. Farrar and K. Worden, "An introduction to structural health monitoring," *Philosophical Transactions of the Royal Society A: Mathematical, Physical and Engineering Sciences*, vol. 365, no. 1851, pp. 303-315, 2007. https://doi.org/10.1098/rsta.2006.1928

[15] F. P. Beer, E. R. Johnston, J. T. DeWolf, and D. F. Mazurek, *Mechanics of materials*, 7th ed. United States: McGraw-Hill Education, 2015.

[16] S. S. Rao, *Mechanical vibrations*, 5th ed. United States: Pearson, 2011.

[17] M. P. Norton and D. G. Karczub, *Fundamentals of noise and vibration analysis for engineers*, 2nd ed. United Kingdom: Cambridge University Press, 2003.

[18] U.S. Department of Defense, *MIL-STD-810H: Environmental engineering considerations and laboratory tests*. United States: U.S. Department of Defense, 2019.

[19] Federal Aviation Administration, *Airworthiness criteria: Special class airworthiness criteria for the Agusta Westland Philadelphia AW609 Powered-Lift. Federal Register*. United States: Federal Aviation Administration, 2024.

[20] H.-r. Fang and D. P. O'Leary, "Euclidean distance matrix completion problems," *Optimization Methods and Software*, vol. 27, no. 4-5, pp. 695-717, 2012. https://doi.org/10.1080/10556788.2011.643888

[21] B. S. Razavi, M. R. Mahmoudkelayeh, and S. S. Razavi, "Damage identification under ambient vibration and unpredictable signal nature," *Journal of Civil Structural Health Monitoring*, vol. 11, pp. 1253-1273, 2021. https://doi.org/10.1007/s13349-021-00503x

Edelweiss Applied Science and Technology
ISSN: 2576-8484
Vol. 9, No. 4: 1176-1189, 2025
DOI: 10.55214/25768484.v9i4.6223